PHYSICAL REVIEW D **92,** 115022 (2015)

Scalar dark matter in light of LEP and proposed ILC experiments

F. Rossi-Torres[*]

Instituto de Física Gleb Wataghin, Universidade Estadual de Campinas—UNICAMP, Rua Sérgio Buarque de Holanda, 777, 13083-859 Campinas, SP, Brazil

C. A. Moura[†]

Centro de Ciências Naturais e Humanas, Universidade Federal do ABC—UFABC, Av. dos Estados, 5001, 09210-580 Santo André, SP, Brazil

(Received 6 May 2015; published 28 December 2015)

In this work we investigate a scalar field dark matter model with mass on the order of 100 MeV. We assume dark matter is produced in the process $e^- + e^+ \to \phi + \phi^* + \gamma$ which, in fact, could be a background for the standard process $e^- + e^+ \to \nu + \bar{\nu} + \gamma$ extensively studied at LEP. We constrain the chiral couplings C_L and C_R of the dark matter with electrons through an intermediate fermion of mass $m_F = 100$ GeV and obtain $C_L = 0.1(0.25)$ and $C_R = 0.25(0.1)$ for the best-fit point of our χ^2 analysis. We also analyze the potential of the International Linear Collider to constrain this scalar dark matter for two configurations: (i) a center-of-mass energy $\sqrt{s} = 500$ GeV and luminosity $\mathcal{L} = 250$ fb^{-1}, and (ii) a center-of-mass energy $\sqrt{s} = 1$ TeV and luminosity $\mathcal{L} = 500$ fb^{-1}. The differences of polarized beams are also explored to better understand the chiral couplings.

DOI: 10.1103/PhysRevD.92.115022 PACS numbers: 95.30.Cq, 12.60.-i, 13.85.Rm

I. INTRODUCTION

Presently, many different sources of data point to the existence of dark matter. In the standard cosmological model, dark matter contributes to the Universe's total energy budget with an energy density of approximately 23.5% [1]. Although we do not know its nature, according to our present knowledge, dark matter must be a new kind of neutral and stable particle [2–4]. Probably, the most well-known kind of hypothesized dark matter particle is the weakly interacting massive particle (WIMP), which is constructed mainly by supersymmetric models. Although several attempts and experimental proposals have been made to detect WIMPs, their existence is not yet confirmed. The observation of a dark matter candidate could be realized once it scatters in nuclei that compound a solid state detector [5]. Examples of this kind of direct-detection experiment are XENON [6], DAMA [7], CoGeNT [8], and CDMS [9].

However, dark matter could be detected in indirect ways such as, for example, annihilation in (i) gamma rays (such as the ones detected in the FermiLAT experiment) [10], (ii) charged particles (explored by PAMELA) [11], (iii) neutrinos (searched for by IceCube) [12], etc. For a review of indirect dark matter searches, see Ref. [13]. Another way to search for dark matter particles is to possibly produce them using colliders. The LHC is an example of a hadronic collider, while LEP [14–23] at CERN or the future International Linear Collider (ILC) [24] are examples of leptonic colliders.

Dark matter models have been explored using LHC data, such as in Refs. [25–28]. This search is mainly based on the dark matter missing energy plus the observed final states from the Higgs decay products. In LEP/ILC, the physical strategy is similar: the annihilation of particles (in this case an electron and a positron) into a pair of dark matter candidates, which are invisible [29]. However, this production can be followed also by a photon that can be detected. In LEP, an excess of events related with dark matter plus monophoton production has not been found beyond the expected background, and limits to such an interaction were placed instead [30,31]. In contrast to previous analyses, we include in our work a dark matter model which takes into account different couplings with right- and left-handed fermions.

Despite the aforementioned experimental efforts, WIMP dark matter remains a hypothesis and its existence is still an ongoing search at the LHC [32]. It is expected that the mass scale of WIMP dark matter is of the order of 100 GeV. However, the authors of Ref. [33] claim that it is possible to have dark matter candidates with masses well below the GeV scale. Other works considered the dark matter particle to be scalar singlet fields [34–38] or more complex models, with different symmetries and other constructions, as explored in Refs. [39–44].

In this study, we analyze a scalar dark matter particle that was explored by Boehm and Fayet [45]. This particle has a mass lighter than $\mathcal{O}(1)$ GeV and couples differently with left- and right-handed fermions. It might be produced in the annihilation of electrons and positrons in the leptonic

[*]ftorres@ifi.unicamp.br
[†]celio.moura@ufabc.edu.br

colliders cited above: LEP and the future ILC. The scalar dark matter model under consideration has four main parameters: (i) one for the coupling with left-chirality leptons, (ii) one for the coupling with right-chirality leptons, (iii) the dark matter mass, and (iv) the mass of a heavy intermediate fermion. We find the constraints in the coupling constants for different intermediate fermion masses. There is no sensitivity to the dark matter mass because the collision energy is much higher than the dark matter mass itself.

This article is organized as follows. In Sec. II we describe the cross section and summarize the model that we test. In Sec. III we present our results for the LEP data (Sec. III A) and make predictions for the ILC (Sec. III B). This section also presents a discussion about the results we obtain. In Sec. IV we conclude our work.

II. PHOTONS PLUS INVISIBLE ENERGY IN e^+e^- COLLIDERS

Consider the interaction

$$e^- + e^+ \to \phi + \phi^* + \gamma, \tag{1}$$

represented by the Feynman diagrams in Fig. 1, where ϕ is the scalar dark matter and ϕ^* is its conjugate with $\phi \neq \phi^*$. These scalar dark matter particles couple to standard model fermions and to a nonstandard intermediate fermion (F). The mass of the fermion F mediating the interaction is typically above $\approx$100 GeV. This is a reasonable assumption, since it is compatible with the nondetection up to now of new charged and heavy fermions. This new nonstandard fermion field may be some mirror partner of other fermions that we know in our Universe. The relevant Feynman rules in our case are expressed by $\phi(C_L\bar{f}_L F_R + C_R\bar{f}_R F_L + \text{H.c.})$, where ϕ is the scalar field dark matter, and C_L and C_R are the Yukawa couplings, respectively, to the left-handed and right-handed standard model fermions. In our analysis, these couplings are free parameters, together with the dark matter mass, m_ϕ, and the mass of the intermediate fermion, m_F. We perform our analysis without showing specific details of the model building, but see Ref. [45] for more details of the model we are considering.

The cross section of the $e^- + e^+ \to \phi + \phi^* + \gamma$ process can be evaluated at tree level using the "radiator approximation" [46]. We present the associated cross section as

$$\sigma(s) = \int dx \int dc_\gamma H(x, s_\gamma; s)\sigma_0(\hat{s}), \tag{2}$$

where s is the square of the center-of-mass energy, and $x = 2E_\gamma/\sqrt{s}$, E_γ is the emitted photon energy. The cross section σ_0 is the cross section associated with the dark matter production by electron-positron annihilation, $e^- + e^+ \to \phi + \phi^*$, written in terms of the parametrized $\hat{s} = s(1-x)$. The total cross section, σ_0, is related to the following differential cross section:

$$\frac{d\sigma_0}{d\Omega} = \left(\frac{1}{8\pi}\right)^2 \frac{|M|^2}{2s} \frac{\sqrt{s/4 - m_\phi^2}}{\sqrt{s/4}}, \tag{3}$$

where Ω is the solid angle and $|M|^2$ is the square amplitude evaluated considering the Feynman diagrams in Fig. 1. The radiator function H is described in the following equation:

$$H(x, s_\gamma; s) = \frac{2\alpha}{\pi x s_\gamma}\left[\left(1 - \frac{x}{2}\right)^2 + \frac{x^2 c_\gamma^2}{4}\right], \tag{4}$$

for $c_\gamma = \cos\theta_\gamma$ and $s_\gamma = \sin\theta_\gamma$, where θ_γ is the photon emission angle.

The radiator function is a good approximation when the emitted photon is neither soft (i.e., with high transverse

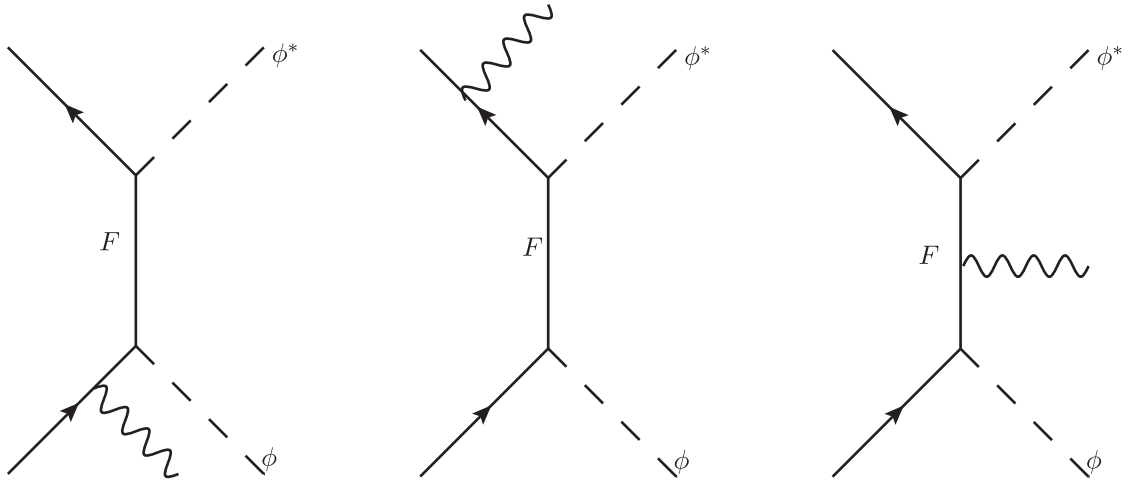

FIG. 1. Relevant Feynman diagrams for the process $e^- + e^+ \to \phi + \phi^* + \gamma$.

momentum) nor collinear to the incoming e^- or e^+. It is important to emphasize that this approximation does not depend on the nature of the electrically neutral particles produced with the photon. This is a reasonable approximation and it works very well for our evaluations. In Fig. 2 of Ref. [47], we find the comparison of the analytical solution and the radiator approximation. It is a very good approximation up to $E_\gamma \approx 450$ GeV ($\sqrt{s} \approx 1$ TeV), which is our most powerful configuration for the ILC (Sec. III B).

We calculate the amplitude for the process $e^- + e^+ \to \phi + \phi^*$, since it can provide information on how relevant the missing energy process can be when compared to the neutrino's missing energy on $e^- + e^+ \to \nu + \bar{\nu}$. Our evaluation takes into account that $m_F \gg m_\phi \gg m_e$. In Fig. 2, for different values of m_F, $C_L = C_R = 0.1$, and $m_\phi = 100$ MeV, we have the total cross section for this process in terms of the center-of-mass energy of the collision, $\sqrt{s}$. From XENON10 data and the fact that dark matter particles with low mass could interact with atomic electrons and ionize these atoms, generating a signal [48], the authors of Ref. [33] obtained the strongest bound on the scattering cross section between dark matter and electrons at a 100 MeV dark matter mass. Although XENON is a direct-detection experiment, this bound at a 100 MeV dark matter mass was a motivation for us to use this value for our scalar dark matter mass.

In order to compare the cross sections (σ_0) of $e^- + e^+ \to \phi + \phi^*$ with the standard model process $e^- + e^+ \to \nu + \bar{\nu}$ ($\sigma_{\rm SM}$), we consider $\sqrt{s} = 100$ GeV as an example. In Fig. 2 we illustrate that (for $m_F = 100$ GeV, $C_L = C_R = 0.1$, and $m_\phi = 100$ MeV) $\sigma_0 \approx 10^{-38}$ cm^2. Using the cross section calculated in Refs. [49,50], $\sigma_{\rm SM} \approx 10^{-35}$ cm^2. So we are clearly describing a subleading process if compared with the electron-positron annihilation into neutrinos.

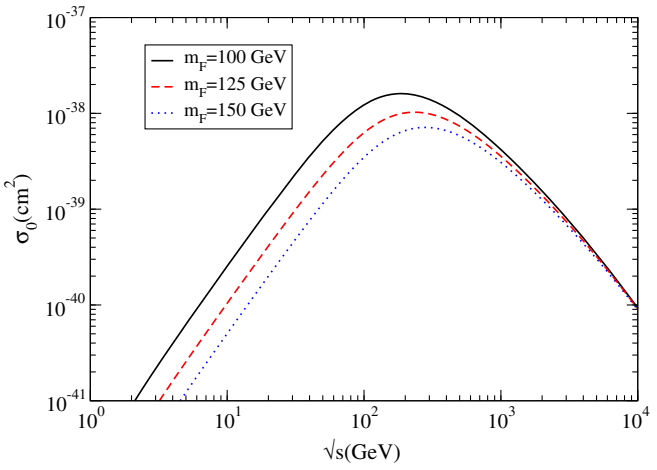

FIG. 2 (color online). Cross section for the process $e^- + e^+ \to \phi + \phi^*$, considering three different fermion masses. The scalar dark matter mass $m_\phi = 100$ MeV and $C_L = C_R = 0.1$.

III. THE PROCESS $e^+e^- \to \phi\phi^*\gamma$ AT LEP AND ILC

We divide this section in two: first, in Sec. III A, we present our results using data from LEP; then, in Sec. III B, we present the ILC potential to investigate dark matter in light of monophoton production from e^+e^- collisions.

A. LEP results

We analyze the possible existence of low-mass dark matter [$\mathcal{O}(100)$ MeV] using LEP data from the experiments [14–23]. The center-of-mass energy $\sqrt{s}$ of the e^+e^- collision varies from 130 to 207 GeV and the luminosity varies from 2.3 to 173.6 pb^{-1}.

We present in Fig. 3 the allowed regions in the $C_L - C_R$ space of parameters for the confidence levels C.L. = 68% (black curves), 90% (red dashed curves), and 95% (blue dotted curves), for $m_F = 100$ GeV and the dark matter mass $m_\phi = 100$ MeV. We find that the χ^2 value increases with m_F. On the other hand, there is no significant variation of the χ^2 value when m_ϕ changes. Actually, the lack of sensitivity with respect to m_ϕ is related to the fact that such a mass is orders of magnitude below the experiment energy scale, $\sqrt{s}$, which is of the order of 100 GeV. The best-fit point for $m_F = 100$ GeV is at $C_L = 0.1$ and $C_R = 0.25$ or at $C_L = 0.25$ and $C_R = 0.1$, with $\chi^2_{\rm min} = 21.97$.

The fact that it is difficult to constrain the dark matter mass with values less than 1 GeV, considering LEP data, was also noticed in Ref. [31]. It is worth noting that the bounds we obtain are compatible with the limits of the annihilation cross section of dark matter candidates that generate the known dark matter abundances. According to Ref. [45], if one considers that $\Omega_\phi h^2 \approx 0.1$, this can be achieved by $C_L C_R \approx 0.01$–0.1 and $m_F \approx 100$–1000 GeV, for any value of m_ϕ less than $\mathcal{O}(1$ GeV$)$.

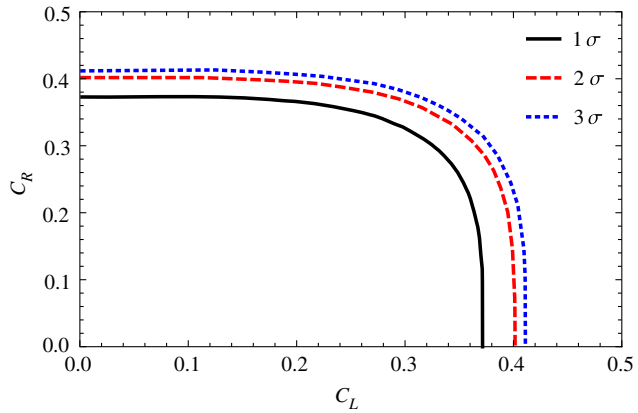

FIG. 3 (color online). Allowed couplings in the parameter space $C_L - C_R$ for 68% (black curves), 90% (red dashed curves), and 95% (blue dotted curves) C.L. $m_F = 100$ GeV and $m_\phi = 100$ MeV. The best-fit point occurs for $C_L = 0.1$ and $C_R = 0.25$ or $C_L = 0.25$ and $C_R = 0.1$.

B. ILC predictions

Identifying the process $e^- + e^+ \to \phi + \phi^* + \gamma$ is a very difficult task, because of the irreducible background from the radiative neutrino production $e^- + e^+ \to \nu + \bar{\nu} + \gamma$. The ILC [24] is expected to have a much higher luminosity and beam polarization than LEP. This increases the possibility to better comprehend the dark matter channel against all possible backgrounds. For instance, it has been shown for WIMP dark matter, with an integrated luminosity of 500 fb^{-1}, that cross sections as small as 12 fb can be observed at the 5σ level, considering only the statistical uncertainty and fully polarized beams [51]. Barthels *et al.* [52] showed that, with a luminosity of 500 fb^{-1}, it is possible to infer the helicity structure of the interaction involved, and the masses and cross sections can be measured with a relative accuracy of the order of 1%.

In order to avoid the collinear and infrared divergences, we impose that $E_\gamma > 8$ GeV and $-0.995 < \cos\theta_\gamma < 0.995$; also, we consider $E_\gamma \leq 220$ GeV when $\sqrt{s} = 500$ GeV and $E_\gamma \leq 450$ GeV for $\sqrt{s} = 1$ TeV, as it was assumed, e.g., in Ref. [53]. These cuts are safe cuts (they avoid a higher background contamination) since there are Z resonances $\sqrt{s}/2(1 - M_z^2/s)$ for the process $e^- + e^+ \to \nu + \bar{\nu} + \gamma$.

As already emphasized, $e^- + e^+ \to \nu + \bar{\nu} + \gamma$ (bg1) is the main contamination channel and its number of events depends on the beam polarization. The second relevant channel of the so-called neutrino background is $e^- + e^+ \to \nu + \bar{\nu} + \gamma + \gamma$ (bg2), where there can be an emission of a second photon, which is not detected. This background channel contributes to about 10% of the total neutrino background. Finally, there is also the Bhabha scattering of leptons with the emission of a photon: $e^- + e^+ \to e^- + e^+ + \gamma$ (bg3). This process can contribute almost the same amount as the neutrino background and it is mostly polarization independent. In Table I we show the number of all relevant background events, taking into account three possible configurations of the beam polarization: (i) unpolarized, i.e., $(P_{e^-}, P_{e^+}) = (0.0, 0.0)$, (ii) $(P_{e^-}, P_{e^+}) = (+0.8, -0.3)$, and (iii) $(P_{e^-}, P_{e^+}) = (-0.8, +0.3)$. All the backgrounds were estimated in Ref. [47] for a luminosity of 1 fb^{-1} and $\sqrt{s} = 500$ GeV. Numbers in parentheses in Table I are the number of background events for the same luminosity, but for $\sqrt{s} = 1$ TeV.

TABLE I. Number of background events from the three different main channels: $e^-e^+ \to \nu + \bar{\nu} + \gamma$ (bg1); $e^- + e^+ \to \nu + \bar{\nu} + \gamma + \gamma$ (bg2); and $e^- + e^+ \to e^- + e^+ + \gamma$ (bg3). The numbers are given for an integrated luminosity of 1 fb^{-1} and $\sqrt{s} = 500\,\text{GeV}\,(1\,\text{TeV})$, considering three different beam polarizations: $(P_{e^-}, P_{e^+}) = (0,0)$ (unpolarized), $(P_{e^-}, P_{e^+}) = (+0.8, -0.3)$, and $(P_{e^-}, P_{e^+}) = (-0.8, +0.3)$. The backgrounds are from Ref. [47].

(P_{e^-}, P_{e^+})	$bg1$	$bg2$	$bg3$
(0, 0)	2257 (2677)	226 (268)	1218 (304)
(+0.8, −0.3)	493 (421)	49 (42)	1218 (304)
(−0.8, +0.3)	5104 (6217)	510 (622)	1218 (304)

The number of background events is modified by the polarization of the beam. This is an important consideration that improves the study of dark matter models at the ILC. The cross section for the dark matter production, σ_0, evaluated using Eq. (3), is also affected. When we consider polarization the cross section (σ_{pol}) is given by [29]

$$\sigma_{\text{pol}} = \frac{1}{4}(1+P_-)[(1+P_+)\sigma_0(e_R^- e_L^+) + (1-P_+)\sigma_0(e_R^- e_R^+)] + \frac{1}{4}(1-P_-)[(1+P_+)\sigma_0(e_L^- e_L^+) + (1-P_+)\sigma_0(e_L^- e_R^+)], \tag{5}$$

where P_- and P_+ are the electron and positron polarizations, respectively. $P_i = 0$ $(i = \pm)$ represents unpolarized beams, and $P_i = 1$ represents a pure right-handed $(i = -)$ electron beam and a left-handed $(i = +)$ positron beam. The $\sigma_0(e_j^- e_k^+)$, $j, k = L, R$, are the cross sections for the different states (left or right) of the electron and positron polarizations in the beam and are evaluated using Eq. (3) and the amplitudes of the Feynman diagrams in Fig. 1. For our process of interest, $e^- + e^+ \to \phi + \phi^* + \gamma$, in the polarized case, we take the value of σ_{pol} now calculated by Eq. (5) and insert it into Eq. (2), substituting σ_0. The procedure of cross section evaluation is very similar to the unpolarized case.

The constraints on the parameters of the model can be evaluated by [54–56]

$$N_{\text{sig}} + N_{\text{bg}} - A\sqrt{N_{\text{sig}} + N_{\text{bg}}} > N_{\text{bg}} + A\sqrt{N_{\text{bg}}}, \tag{6}$$

where $A = 1.64$ for the 95% confidence level, and N_{sig} and N_{bg} are, respectively, the number of signal events and background events after considering all the cuts.

Figure 4 illustrates the bounds for C_L and C_R at 95% C.L., considering $m_\phi = 100$ MeV, $\sqrt{s} = 500$ GeV, and $\mathcal{L} = 250$ fb^{-1}, for three different values of m_F: $m_F = 100$ GeV (black solid line), $m_F = 200$ GeV (blue dotted line), and $m_F = 300$ GeV (red dashed line). These values are evaluated for an unpolarized beam.

As in the LEP case, a variation in the dark matter mass does not affect the constraints, since $\sqrt{s} \gg m_\phi$. We found that, for $m_F = 100$ GeV, we obtain better constraints, which is expected with the increased luminosity. The ILC can provide, roughly speaking, coupling constraints that are 4 times stricter than LEP in similar conditions. For an ILC configuration of $\sqrt{s} = 1$ TeV and $\mathcal{L} = 500$ fb^{-1} (dashed curve in Fig. 5), $C_L - C_R$ coupling parameters are more constrained than for the configuration of $\sqrt{s} = 500$ GeV and $\mathcal{L} = 250$ fb^{-1} (solid curve). Both curves

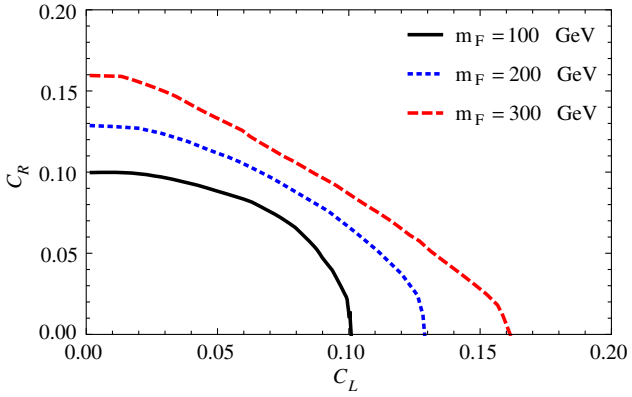

FIG. 4 (color online). Bounds at 95% C.L. on the $C_L - C_R$ couplings considering $m_\phi = 100$ MeV, $\sqrt{s} = 500$ GeV, and $\mathcal{L} = 250$ fb^{-1}. The black solid curve is for $m_F = 100$ GeV, the blue dotted line is for $m_F = 200$ GeV, and the red dashed line is for $m_F = 300$ GeV.

were obtained considering $m_\phi = 100$ MeV and $m_F = 100$ GeV. We observe this behavior—when the energy of the collision as well as the luminosity of the experiment increases—due to a slight reduction of the background events and an increase of events in the dark matter channel production (Table I). Although the cross section for the process is reduced when the collision energy increases, this reduction is not significant when compared with the increase in the luminosity.

We also calculated the results by taking into account two configurations for the polarization of the beam: $(P_{e^-}, P_{e^+}) = (+0.8, -0.3)$ and $(P_{e^-}, P_{e^+}) = (-0.8, +0.3)$. Figure 6 represents the 95% C.L. on the $C_L - C_R$ couplings

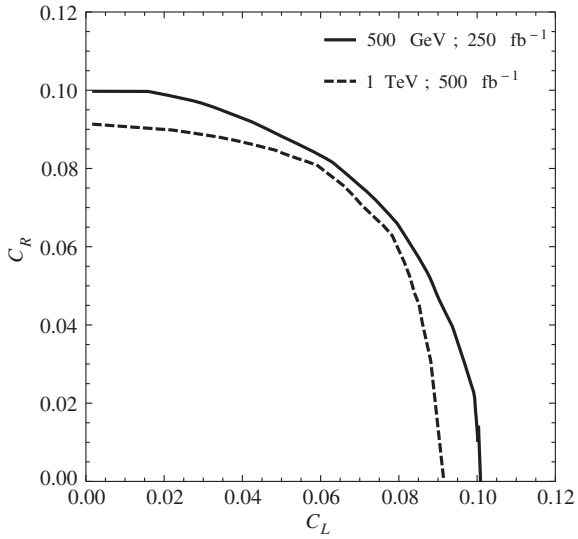

FIG. 5. Bounds at 95% C.L. on the $C_L - C_R$ couplings considering $m_\phi = 100$ MeV and $m_F = 100$ GeV. The solid curve is for the ILC with $\sqrt{s} = 500$ GeV and $\mathcal{L} = 250$ fb^{-1}, and the dashed curve is for the ILC with $\sqrt{s} = 1$ TeV and $\mathcal{L} = 500$ fb^{-1}.

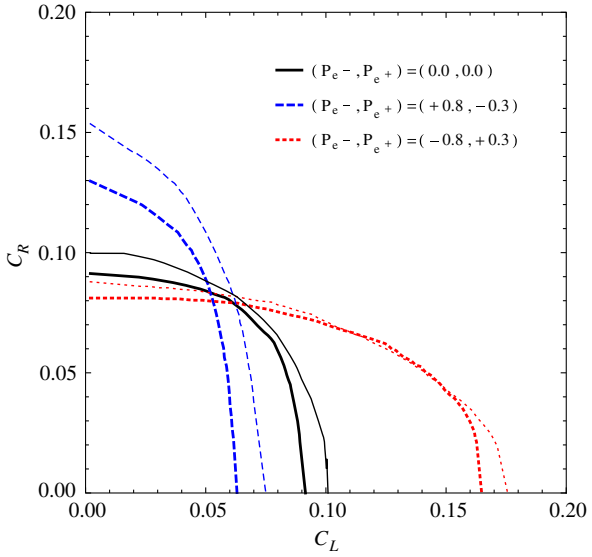

FIG. 6 (color online). Bounds at 95% C.L. on the $C_L - C_R$ couplings considering $m_\phi = 100$ MeV and $m_F = 100$ GeV. The ILC configuration has been set for $\sqrt{s} = 500$ GeV and $\mathcal{L} = 250$ fb^{-1}. The black solid line is for an unpolarized beam, the blue dashed line is for $(P_{e^-}, P_{e^+}) = (+0.8, -0.3)$, and the red dotted line is for $(P_{e^-}, P_{e^+}) = (-0.8, +0.3)$. The thinner lines for $\sqrt{s} = 500$ GeV and $\mathcal{L} = 250$ fb^{-1} and the thicker lines for $\sqrt{s} = 1$ TeV and $\mathcal{L} = 500$ fb^{-1}.

considering $m_\phi = 100$ MeV and $m_F = 100$ GeV. The black solid line is for an unpolarized beam, the blue dashed line is for $(P_{e^-}, P_{e^+}) = (+0.8, -0.3)$, and the red dotted line is for $(P_{e^-}, P_{e^+}) = (-0.8, +0.3)$. The thinner (upper) lines represent the ILC configuration of $\sqrt{s} = 500$ GeV and $\mathcal{L} = 250$ fb^{-1} and the thicker lines exemplify the ILC configuration of $\sqrt{s} = 1$ TeV and $\mathcal{L} = 500$ fb^{-1}.

As already mentioned and presented in Fig. 5, a greater luminosity in the experiment imposes a more constrained region of the space of parameters. As expected, when we consider the beam polarization, asymmetries in the curves appear. As noticed in Fig. 6, the polarization configuration of the blue dashed line is almost a rotated version of the red dotted curve, since there is an inversion of the beam polarization: $(P_{e^-}, P_{e^+}) = (+0.8, -0.3) \to (P_{e^-}, P_{e^+}) = (-0.8, +0.3)$. Differences between these two curves are related to the number of background events when we modify the polarization, as represented in Table I.

The potential of the ILC to investigate processes like those we described here depends on various unknowns aspects: the trigger; the amount of data taken with this monophoton trigger process; cut efficiencies; and the comprehension of the background rate and the capability to estimate the background. We performed a more simplified analysis of our space parameter, but in order to really explore the potential of the ILC experiment to discover scalar dark matter it would be necessary to perform future Monte Carlo simulations, combined with detector

simulation and event reconstruction for the parameters related with the signal. These future procedures, together with direct and indirect approaches, are main keys to exploring and better understanding the unknown dark matter particles.

IV. CONCLUSIONS

In this work, we analyzed data from LEP in the context of a scalar dark matter model. The production of the dark matter particle, $e^- + e^+ \to \phi + \phi^* + \gamma$, was confronted with other standard model backgrounds, such as $e^- + e^+ \to \nu + \bar{\nu} + \gamma$. We constrained the C_L and C_R couplings for an intermediate heavy fermion mass $m_F = 100$ GeV and dark matter mass $m_\phi = 100$ MeV. We obtained $C_L = 0.1(0.25)$ and $C_R = 0.25(0.1)$ as best-fit points. When m_F increases, χ^2 becomes inaccurate and unresponsive to the dark matter mass (m_ϕ). We also investigated the potential of the ILC to constrain scalar field dark matter models. Using an unpolarized beam and $E_\gamma \leq 220$ GeV when we consider $\sqrt{s} = 500$ GeV and $\mathcal{L} = 250$ fb^{-1}, and $E_\gamma \leq 450$ GeV for $\sqrt{s} = 1$ TeV and $\mathcal{L} = 500$ fb^{-1}, it is clear that the ILC is more sensitive than LEP to investigate scalar field dark matter models, since it will have a greater luminosity, polarization information, and an improved comprehension of the backgrounds.

Although the ILC has no sensitivity for m_ϕ, since $\sqrt{s} \gg m_\phi$, it can have different polarization configurations. There is great potential to explore models where there are distinctions in couplings between dark matter with left- and right-handed fermions, as seen in Fig. 6. Our study signalizes the importance to deeply explore dark matter and broken chiral symmetry models and the potential to accomplish this at the future ILC or any other future electron-positron collider. It opens the possibility to study models that contain a large spectrum of dark matter masses and to explore nonstandard weak couplings, such as those found in Refs. [57–62], among many other works on the subject. Lepton colliders are very important tests for dark matter, since backgrounds can, in principle, be much better understood and provide clearer event signals.

ACKNOWLEDGMENTS

F. R.-T. would like to thank Conselho Nacional de Desenvolvimento Científico e Tecnológico (CNPq) for financial support (Grant No. 150102/2013-5). The work of C. A. M. was partially supported by Fundação de Amparo à Pesquisa do Estado de São Paulo (FAPESP), under the Grant No. 2013/22079-8. The authors would like to thank O. L. G. Peres for the suggestion of the subject we have developed here.

[1] G. Hinshaw *et al.* (WMAP Collaboration), Nine-year wilkinson microwave anisotropy probe (WMAP) observations: Cosmological parameter results, Astrophys. J. Suppl. Ser. **208**, 19 (2013).
[2] G. Jungman, M. Kamionkowski, and K. Griest, Supersymmetric dark matter, Phys. Rep. **267**, 195 (1996).
[3] L. Bergstrom, Non-baryonic dark matter: Observational evidence and detection methods, Rep. Prog. Phys. **63**, 793 (2000).
[4] G. Bertone, D. Hooper, and J. Silk, Particle dark matter: Evidence, candidates and constraints, Phys. Rep. **405**, 279 (2005).
[5] K. Freese, M. Lisanti, and C. Savage, Colloquium: Annual modulation of dark matter, Rev. Mod. Phys. **85**, 1561 (2013).
[6] E. Aprile *et al.* (XENON100 Collaboration), Dark Matter Results from 225 Live Days of XENON100 Data, Phys. Rev. Lett. **109**, 181301 (2012); The XENON100 dark matter experiment, Astropart. Phys. **35**, 573 (2012).
[7] R. Bernabei *et al.* (DAMA and LIBRA Collaborations), New results from DAMA/LIBRA, Eur. Phys. J. C **67**, 39 (2010).
[8] C. E. Aalseth *et al.* (CoGeNT Collaboration), CoGeNT: A search for low-mass dark matter using p-type point contact germanium detectors, Phys. Rev. D **88**, 012002 (2013).
[9] Z. Ahmed *et al.* (CDMS-II Collaboration), Results from a Low-Energy Analysis of the CDMS II Germanium Data, Phys. Rev. Lett. **106**, 131302 (2011).
[10] M. Ackermann *et al.* (LAT Collaboration), Fermi LAT search for dark matter in gamma-ray lines and the inclusive photon spectrum, Phys. Rev. D **86**, 022002 (2012).
[11] L. Bergstrom, T. Bringmann, and J. Edsjo, New positron spectral features from supersymmetric dark matter: A way to explain the PAMELA data?, Phys. Rev. D **78**, 103520 (2008); V. Barger, W. Y. Keung, D. Marfatia, and G. Shaughnessy, PAMELA and dark matter, Phys. Lett. B **672**, 141 (2009); F. Donato, D. Maurin, P. Brun, T. Delahaye, and P. Salati, Constraints on WIMP Dark Matter from the High Energy PAMELA $\bar{p}/p$ Data, Phys. Rev. Lett. **102**, 071301 (2009).
[12] M. G. Aartsen *et al.* (IceCube Collaboration), IceCube search for dark matter annihilation in nearby galaxies and galaxy clusters, Phys. Rev. D **88**, 122001 (2013); Search for Dark Matter Annihilations in the Sun with the 79-String IceCube Detector, Phys. Rev. Lett. **110**, 131302 (2013).
[13] M. Cirelli, Indirect searches for dark matter, Pramana **79**, 1021 (2012).
[14] R. Barate *et al.* (ALEPH Collaboration), Search for supersymmetry in the photon(s) plus missing energy channels at $\sqrt{s} = 161$ GeV and 172 GeV, Phys. Lett. B **420**, 127 (1998).

[15] R. Barate *et al.* (ALEPH Collaboration), Single- and multi-photon production in e^+e^- collisions at a centre-of-mass energy of 183 GeV, Phys. Lett. B **429**, 201 (1998).
[16] A. Heister *et al.* (ALEPH Collaboration), Single- and multi-photon production in ee collisions at $\sqrt{s}$ up to 209 GeV, Eur. Phys. J. C **28**, 1 (2003).
[17] P. Abreu *et al.* (DELPHI Collaboration), Photon events with missing energy at $\sqrt{s} = 183$ to 189 GeV, Eur. Phys. J. C **17**, 53 (2000).
[18] M. Acciarri *et al.* (L3 Collaboration), Single and multi-photon events with missing energy in e^+e^- collisions at 161 GeV $< \sqrt{s} <$ 172 GeV, Phys. Lett. B **415**, 299 (1997).
[19] M. Acciarri *et al.* (L3 Collaboration), Single and multi-photon events with missing energy in e^+e^- collisions at $\sqrt{s} = 183$ GeV, Phys. Lett. B **444**, 503 (1998).
[20] M. Acciarri *et al.* (L3 Collaboration), Single and multi-photon events with missing energy in e^+e^- collisions at $\sqrt{s} = 189$ GeV, Phys. Lett. B **470**, 268 (1999).
[21] K. Ackerstaff *et al.* (OPAL Collaboration), Search for anomalous production of photonic events with missing energy in e^+e^- collisions at $\sqrt{s} = 130$–172 GeV, Eur. Phys. J. C **2**, 607 (1998).
[22] G. Abbiendi *et al.* (OPAL Collaboration), Search for anomalous photonic events with missing energy in e^+e^- collisions at $\sqrt{s} = 130, 136$ and 183 GeV, Eur. Phys. J. C **8**, 23 (1999).
[23] G. Abbiendi *et al.* (OPAL Collaboration), Photonic events with missing energy in e^+e^- collisions at $\sqrt{s} = 189$ GeV, Eur. Phys. J. C **18**, 253 (2000).
[24] ILC Collaboration, Report No. ILC-REPORT-2007-001.
[25] A. Askew, S. Chauhan, B. Penning, W. Shepherd, and M. Tripathi, Searching for dark matter at hadron colliders, Int. J. Mod. Phys. A **29**, 1430041 (2014).
[26] A. Berlin, T. Lin, and L.-T. Wang, Mono-Higgs detection of dark matter at the LHC, J. High Energy Phys. 06 (2014) 078.
[27] A. A. Petrov and W. Shepherd, Searching for dark matter at LHC with mono-Higgs production, Phys. Lett. B **730**, 178 (2014).
[28] L. Carpenter, A. DiFranzo, M. Mulhearn, C. Shimmin, S. Tulin, and D. Whiteson, Mono-Higgs-boson: A new collider probe of dark matter, Phys. Rev. D **89**, 075017 (2014).
[29] A. Birkedal, K. Matchev, and M. Perelstein, Dark matter at colliders: A model-independent approach, Phys. Rev. D **70**, 077701 (2004).
[30] P. J. Fox, R. Harnik, J. Kopp, and Y. Tsai, LEP shines light on dark matter, Phys. Rev. D **84**, 014028 (2011).
[31] R. Essig, J. Mardon, M. Papucci, T. Volansky, and Y.-M. Zhong, Constraining light dark matter with low-energy e^+e^- colliders, J. High Energy Phys. 11 (2013) 167.
[32] G. Bertone, The moment of truth for WIMP dark matter, Nature (London) **468**, 389 (2010).
[33] R. Essig, A. Manalaysay, J. Mardon, P. Sorensen, and T. Volansky, First Direct Detection Limits on Sub-GeV Dark Matter from XENON10, Phys. Rev. Lett. **109**, 021301 (2012).
[34] V. Silveira and A. Zee, Scalar Phantoms, Phys. Lett. **161B**, 136 (1985).
[35] J. McDonald, Gauge singlet scalars as cold dark matter, Phys. Rev. D **50**, 3637 (1994).
[36] C. P. Burgess, M. Pospelov, and T. ter Veldhuis, The minimal model of nonbaryonic dark matter: A singlet scalar, Nucl. Phys. **B619**, 709 (2001).
[37] T. Matos and R. Lopez-Fernandez, A SM singlet scalar as Dark Matter, arXiv:1403.5243.
[38] M. Kadastik, K. Kannike, A. Racioppi, and M. Raidal, Implications of the 125 GeV Higgs boson for scalar dark matter and for the CMSSM phenomenology, J. High Energy Phys. 05 (2012) 061.
[39] O. Fischer and J. J. van der Bij, The scalar singlet-triplet dark matter model, J. Cosmol. Astropart. Phys. 01 (2014) 032.
[40] E. Gabrielli, M. Heikinheimo, K. Kannike, A. Racioppi, M. Raidal, and C. Spethmann, Towards completing the standard model: Vacuum stability, electroweak symmetry breaking, and dark matter, Phys. Rev. D **89**, 015017 (2014).
[41] S. Baek, P. Ko, and W.-I. Park, Local Z_2 scalar dark matter model confronting galactic GeV-scale γ-ray, Phys. Lett. B **747**, 255 (2015).
[42] E. C. F. S. Fortes, A. C. B. Machado, J. Montao, and V. Pleitez, Scalar dark matter candidates in a two inert Higgs doublet model, J. Phys. G **42**, 105003 (2015).
[43] C. J. Lee and J. Tandean, Lepton-flavored scalar dark matter with minimal flavor violation, J. High Energy Phys. 04 (2015) 174.
[44] D. Cogollo, A. X. Gonzalez-Morales, F. S. Queiroz, and P. R. Teles, Excluding the light dark matter window of a 331 model using LHC and direct dark matter detection data, J. Cosmol. Astropart. Phys. 11 (2014) 002.
[45] C. Boehm and P. Fayet, Scalar dark matter candidates, Nucl. Phys. **B683**, 219 (2004).
[46] O. Nicrosini and L. Trentadue, Structure function approach to the neutrino counting problem, Nucl. Phys. **B318**, 1 (1989).
[47] H. K. Dreiner, M. Huck, M. Kramer, D. Schmeier, and J. Tattersall, Illuminating dark matter at the ILC, Phys. Rev. D **87**, 075015 (2013).
[48] R. Essig, J. Mardon, and T. Volansky, Direct detection of sub-GeV dark matter, Phys. Rev. D **85**, 076007 (2012).
[49] G. 't Hooft, Prediction for neutrino-electron cross-sections in Weinberg's model of weak interactions, Phys. Lett. **37B**, 195 (1971).
[50] D. A. Dicus, Stellar energy-loss rates in a convergent theory of weak and electromagnetic interactions, Phys. Rev. D **6**, 941 (1972).
[51] K. Murase, T. Tanabe, T. Suehara, S. Yamashita, and S. Komamiya, Using single photons for WIMP searches at the ILC, arXiv:1006.3551.
[52] C. Bartels, M. Berggren, and J. List, Characterising WIMPs at a future e^+e^- linear collider, Eur. Phys. J. C **72**, 2213 (2012).
[53] K. Kadota and J. Silk, Constraints on light magnetic dipole dark matter from the ILC and SN 1987A, Phys. Rev. D **89**, 103528 (2014).
[54] N. Brown, Degenerate Higgs and Z Boson at LEP200, Z. Phys. C **49**, 657 (1991).
[55] H. Baer, M. Bisset, C. Kao, and X. Tata, Observability of $\gamma\gamma$ decays of Higgs bosons from supersymmetry at hadron supercolliders, Phys. Rev. D **46**, 1067 (1992).

[56] C. Kao, D. A. Dicus, R. Malhotra, and Y. Wang, Discovering the Higgs bosons of minimal supersymmetry with tau leptons and a bottom quark, Phys. Rev. D **77**, 095002 (2008).

[57] A. Alves, E. Ramirez Barreto, D. A. Camargo, and A. G. Dias, A model with chiral quarks of electric charges $-4/3$ and $5/3$, J. High Energy Phys. 07 (2013) 129.

[58] J. Alwall and J. Tandean, Heavy chiral fermions and dark matter, Adv. High Energy Phys. **2013**, 915897 (2013).

[59] R. Essig, Direct detection of nonchiral dark matter, Phys. Rev. D **78**, 015004 (2008).

[60] T. Cohen, J. Kearney, A. Pierce, and D. Tucker-Smith, Singlet-doublet dark matter, Phys. Rev. D **85**, 075003 (2012).

[61] A. Alves, S. Profumo, and F. S. Queiroz, The dark Z' portal: direct, indirect and collider searches, J. High Energy Phys. 04 (2014) 063.

[62] A. Alves, A. Berlin, S. Profumo, and F. S. Queiroz, Dark matter complementarity and the Z' portal, Phys. Rev. D **92**, 083004 (2015).